AUT Journal of Electrical Engineering

AUT J. Elec. Eng., 50(2) (2018) 109-120
DOI: 10.22060/eej.2018.14303.5217

Model Predictive Control of Distributed Energy Resources with Predictive Set-Points for Grid-Connected Operation

A. Saleh*, A. Deihimi

Electrical Engineering Department, Bu-Ali Sina University, Hamedan, Iran

ABSTRACT: This paper proposes an MPC - based (model predictive control) scheme to control active and reactive powers of DERs (distributed energy resources) in a grid - connected mode (either through a bus with its associated loads as a PCC (point of common coupling) or an MG (micro - grid)). DER may be a DG (distributed generation) or an ESS (energy storage system). In the proposed scheme, the set - points provided to MPC are forecast for future instances by a linear extrapolation to gain smooth active and reactive power exchange under various loading conditions (e.g. balanced / imbalanced, nonlinear and dynamic loading) and voltage imbalance imposed by the upstream grid. In this scheme active and reactive power control change to current control and the references of the currents are forecast. The stability of the proposed control scheme is analyzed and discussed. The effectiveness of the proposed scheme is demonstrated by extensive time - domain simulations using PSCAD / EMTDC for various conditions (various loads, voltage imbalance, parallel operation with other DGs, parameter uncertainties and measurement noises) in several case studies. Comparing the obtained results with those of the two other schemes (PI - based and convectional MPC) shows the superiority of the proposed scheme.

Review History:

Received: 9 April 2018
Revised: 10 June 2018
Accepted: 4 September 2018
Available Online: 1 October 2018

Keywords:
Distributed Energy Resource
Micro-Grid
Grid-Connected Operation
Model Predictive Control
Predictive Set-Points

1- Introduction

MGs (micro-grids) which consist of DERs (distributed energy resources) (DGs (distributed generations) and ESSs (energy storage systems)) and loads, which are electrically connected to each other, are conceived as a small grid [1], [2]. As DGs, WT (wind turbine) and PV (photovoltaic array) are suitable to apply in MGs, because of their geographical small size and more scalable than conventional power plants. Also, conventional generators (diesel and gas fueled generators) are used into MGs [3]. When WT and PV are used as the major DGs in the MGs, since energy sources of them have intermittent and stochastic nature, energy storages, as ESSs, play an important role in the MGs to support renewable power penetrations [4]. MG can operate grid-connected or islanded. In grid-connected operation, MG is connected to the main grid at the PCC (point of common coupling) and voltage and frequency are dictated by the main grid. In this operation mode DERs must properly exchange active and reactive powers that are deduced by operation management [5] in the various conditions e.g. imbalanced/nonlinear load and imposed voltage imbalance. In reference [6], a current-controlled real-/reactive-power controller is developed where conventional PI-based is used as the main controller. This control scheme is designed for inverter-based renewable sources which are connected to a balanced grid and has no proper performance under unmoral conditions. References [7] and [8] proposed direct power control strategies based on sliding mode control method under voltage unbalancing of main grid, but imbalanced/nonlinear load conditions are not demonstrated. Two control schemes based on adaptive Lyapunov function and sliding mode method in [9] are used to compensate the negative-sequence current components caused by unbalanced loads in some part of the MG and directly regulate the positive-sequence active and reactive power injected by DGs to the MG, respectively. Reference [10] proposed direct Lyapunov control method to control DGs in a grid connected MG with nonlinear loads. The used method in [11] is developed to improve grid-connected operation of inverter-based renewable resources under grid-impedance uncertainties. The proposed control scheme in [12] utilizes PI current controller for a WT to control delivered power to distributed grid under existence nonlinear loads.

In recent years, MPC (model predictive control) has found many applications in power electronics and other industrial fields [13-23]. MPC is greatly suitable for the control of power converters due to its fast dynamic response, easy inclusion of nonlinearities and flexibility to include system requirements in controller design [19]. One of the solutions to control the grid-connected electronically-interfaced DGs was proposed in [13] where a direct power control scheme based on MPC was designed and examined for normal conditions, e.g. balanced load and grid voltage and imbalanced/nonlinear load and voltage imbalance conditions were not considered. Model predictive scheme was proposed in [14] to control active and reactive powers for a single WT connected to the main grid through an LC filter. This reference considered neither imbalanced/nonlinear load nor voltage imbalance conditions.

In view of the aforementioned previous works, the main controller of inverter-based DERs should be preferably designed insensitive to loading dynamics to give a robust transient and steady-state performance at various loading and bus voltage conditions under grid-connected operation. Moreover, the fast dynamic response of MPC along with its optimal dedicated design based on system requirements can be used to achieve better regulation of power exchange of

Corresponding author, E-mail: hosein.saleh@chmail.ir

a DER with on-grid system. Hence, a control scheme based on MPC is proposed in this paper for the main controller of inverter-based DERs where set-points of the inverter currents are forecast for future times (against conventional method in design of MPC) to give a desired performance regardless of loading variations or bus voltage imbalance. The effectiveness of the proposed control scheme is demonstrated by time-domain simulation conducted in PSCAD/EMTDC.

This paper is organized as follows. In section 2, the considered multi-bus MG is described. Structure of used DERs in the MG and their main proposed controllers are developed in sections 3 and 4. Simulation results are discussed in section 5, and conclusion is given in section 6.

2- Multi-bus MG description

Fig.1 shows the single-line diagram of the considered multi-bus MG.

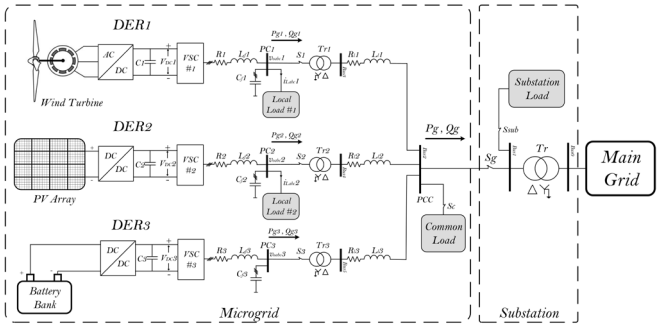

Fig. 1. Single-line diagram of the considered multi-bus MG.

The MG consists of three inverter-based DER units which two of them are DGs and the other is ESS. DER1 is a WT, and DER2 is a PV array. WT and PV are main producers. The DER3 is a BT (battery bank) for storing extra energy produced by DGs or receiving from main grid in off-peak durations. The stored energy is used when DGs cannot provide power demand. Voltage of DER converter dc-link is regulated by its respective AC/DC or DC/DC converter at a desired voltage (V_{DC}) as seen in Fig. 1, and the DER will deliver the necessary power in such a way that maintains the power balance in the dc-link [22]. Thus the energy source/storage of each DER is replaced by an ideal DC voltage source [24]. Each DER is connected to its PC (point of connection) bus through an LC filter. Power exchange of each DER is occurred through a step-up Y/Δ transformer. Transformers are paralleled to each other at PCC (point of common coupling) through interlink-lines modeled by series *RL* branches. PCC is connected to 20 *KV* main grid via a step-up Δ/Y transformer (as main transformer) installed in substation. Three groups of loads are assumed that includes local load, common load and substation load. Local loads are connected to PC buses of DGs. This group (Fig.2) consists of balanced/imbalanced, nonlinear and dynamic motor loads. Common load which is a balanced load is connected to PCC. Substation load is connected to the low voltage side of the main transformer that can be balanced/imbalanced load. Parameters of the DERs, MG, substation and main grid are given in Table 1.

Table 1. DERs, MG, Substation and Main Grid parameters

Parameter		Remark
DERs		
Power rating	10	Inverter
L_f	100	filter
C_f	500	
R	1.5	
V_{DC}	4	DC-link
f_s	6480	Switching frequency
Ts [μs]	10	Sampling time
Tr	0.612/4 (Y/Δ)	Leakage reactance X=10%
Local Loads		
R_1	83	RL *Local* Load
L_1	137	
R_2	50	RLC *Local* Load
L_2	68	
C_2	13.55	
R_3	17	Imbalanced *Local* Load (phase *a* to ground- Tr: 0.612/0.184 (Δ /Y), X=10%)
L_3	21.8	
R_4	700	Nonlinear *Local* Load (Tr: 0.612/0.612 (Δ /Y), X=10%)
L_4	20	
Power rating	0.8	Induction Machine *Local* Load
V_m	0.868	
ω	377	
R_r [pu]	0.0132	
R_s [pu]	0.0184	
L_m [pu]	3.8	
L_{lr} [pu]	0.0223	
L_{ls} [pu]	0.0223	
MG		
Z_{l1}	50+j37.70	Inter-link lines Impedance
Z_{l2}	60+j45.24	
Z_{l3}	55+j41.47	
R_c	8300	RL *Common* Load
L_c	13700	
Substation		
Tr	4/20 (Δ /Y)	Leakage reactance X=10%
R_{sub}	7	Imbalanced *Substation* Load (phase *a* to ground- Tr: 4/0.612 (Δ /Y), X=10%)
L_{sub}	20	
Main Grid		
V	20	

Power rating [MVA], Z [mΩ], R [mΩ], L [μH], V [kV], ω [rad/sec], f_s [Hz]

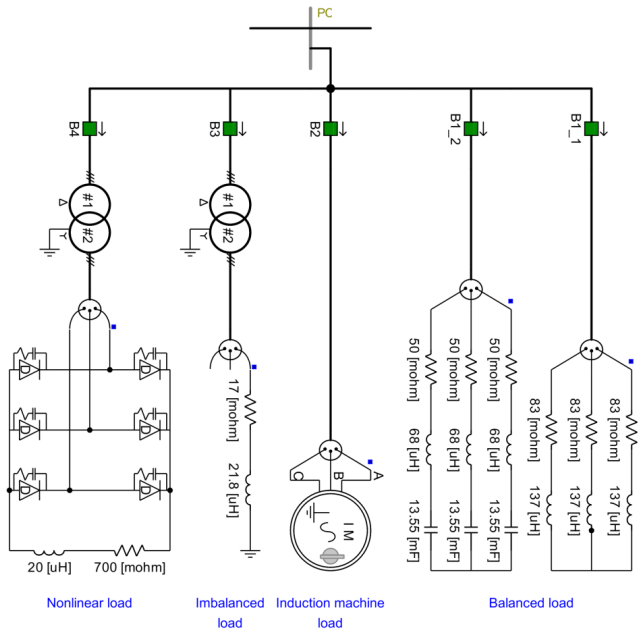

Fig. 2. The collection of different load types connected to the PC of the DGs.

3- DER and its main controller

A typical inverter-based DER along with its main controller is shown in Fig. 3. The synchronous *dq* reference frame is used for the control system while the PLL (phase locked loop) [25] produces ρ as the angle between the rotating *d*-axis and the stationary α-axis as well as ω as the angular frequency of PC voltage. PC voltage v_{oabc} and ω are imposed by the upstream grid.

The main controller regulates exchanged active and reactive powers to their set-points (P_g^*, Q_g^*). For DGs, P_g^* is determined by the MPPT (maximum power point tracker) algorithm [26-29], and for ESS, is deduced based on power balance as follow [5]:

$$P_{WT} + P_{PV} + P_{BT} = P_{loss} + P_{load} + P_{demand} \tag{1}$$

P_{WT}, P_{PV} and P_{BT} are WT, PV and BT powers. P_{loss}, P_{load} and P_{demand} are total loss of the MG network, total load in MG and demanded power by main grid.

Q_g^* is provided by the MG operator that can be zero, negative or positive values [14]. The instantaneous active and reactive powers P_g and Q_g are exchanged between DER and upstream grid, calculated from output voltages and currents as bellow

$$P_g(t) = \frac{3}{2}(v_{od}(t)i_{gd}(t) + v_{oq}(t)i_{gq}(t)) \tag{2}$$

$$Q_g(t) = \frac{3}{2}(-v_{od}(t)i_{gq}(t) + v_{oq}(t)i_{gd}(t)) \tag{3}$$

v_{od} and v_{oq} are *dq* components of the PC voltage. i_{gd}, and i_{gq} are *dq* components of the interlink-line currents. With respect to (2) and (3), one can deduce that [6]

$$i_{gd}^*(t) = \frac{2}{3}\frac{V_{od}(t)}{V_{od}^2(t)+V_{oq}^2(t)}P_g^*(t) + \frac{2}{3}\frac{V_{oq}(t)}{V_{od}^2(t)+V_{oq}^2(t)}Q_g^*(t) \tag{4}$$

$$i_{gq}^*(t) = \frac{2}{3}\frac{V_{oq}(t)}{V_{od}^2(t)+V_{oq}^2(t)}P_g^*(t) - \frac{2}{3}\frac{V_{od}(t)}{V_{od}^2(t)+V_{oq}^2(t)}Q_g^*(t) \tag{5}$$

where V_{od} and V_{oq} are signals obtained from filtering v_{od} and v_{oq} respectively. i_{gd}^*, and i_{gq}^* are set-points of i_{gd} and i_{gq} respectively. v_{od} and v_{oq} are filtered in such a way that only high frequency disturbances caused by inverter switching can be removed. Thus, tracking the P_g^* and Q_g^* are changed to tracking the i_{gd}^* and i_{gq}^*. In the next section the proposed control scheme is described.

4- The proposed control scheme

4- 1- Controller construction

In this section, MPC [30] is used for the main controller of an inverter-based DER to regulate i_{gd} and i_{gq} of the DER connected to an on-grid system (Fig.3). Assume that a DER is individually connected to a balanced main grid (v_{od} = dc constant and v_{oq} = 0) and has no local load (i_{Labc} = 0). With respect to Fig.3 [6]

$$i_d(t) = i_{gd}(t) \tag{6}$$

$$i_q(t) = i_{gq}(t) + C_f\omega v_o \tag{7}$$

Therefore, in order to control $i_{gd}(t)$ and $i_{gq}(t)$, $i_d(t)$ and $i_q(t)$ must be controlled. $i_d(t)$ and $i_q(t)$ are *dq* components of the inverter currents. Thus state-space equations of the model can be expressed as given in (8)-(10).

$$\dot{\boldsymbol{x}}(t) = \boldsymbol{A}_c\boldsymbol{x}(t) + \boldsymbol{B}_c\boldsymbol{u}(t) + \boldsymbol{D}_c\boldsymbol{d}(t) \tag{8}$$

$$\boldsymbol{x} = \begin{bmatrix} i_d \\ i_q \end{bmatrix}, \boldsymbol{u} = \begin{bmatrix} m_d \\ m_q \end{bmatrix}, \ \boldsymbol{d} = \begin{bmatrix} v_d \\ v_q \end{bmatrix} \tag{9}$$

$$\boldsymbol{A}_c = \begin{bmatrix} -\frac{R}{L_f} & \omega \\ -\omega & -\frac{R}{L_f} \end{bmatrix}, \ \boldsymbol{B}_c = \begin{bmatrix} \frac{1}{L_f}\frac{V_D}{2} & 0 \\ 0 & \frac{1}{L_f}\frac{V_D}{2} \end{bmatrix}, \ \boldsymbol{D}_c = \begin{bmatrix} -\frac{1}{L_f} & 0 \\ 0 & -\frac{1}{L_f} \end{bmatrix} \tag{10}$$

$\boldsymbol{x}$, $\boldsymbol{u}$ and $\boldsymbol{d}$ are vectors of states, inputs and disturbances, respectively. m_d and m_q are *dq* components of modulating signals. Filter inductance and capacitance are denoted by L_f and C_f, respectively. R models the ohmic loss of the filter inductor and includes the effects of on-state resistance of switches. The states of the model are also assumed as the

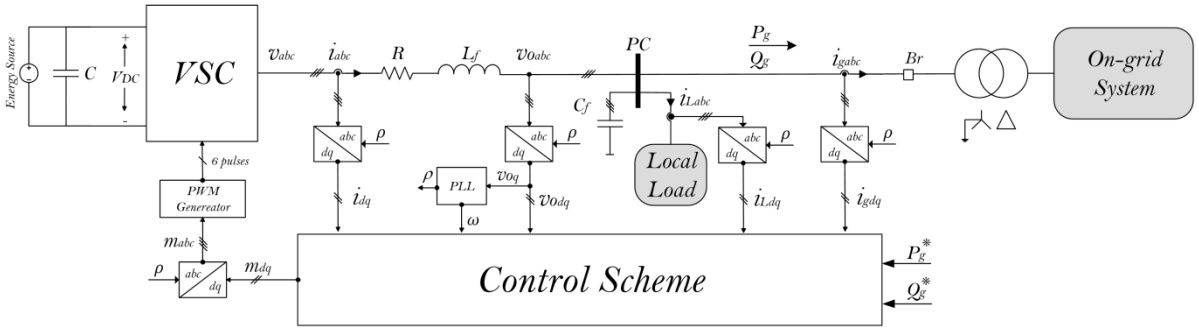

Fig. 3. A typical inverter-based DER along with its main controller

outputs of the model as given in (11) and (12) in order to limit the excursions of output currents of the inverter in design of MPC.

$$\boldsymbol{y}(t) = \boldsymbol{C}_c \boldsymbol{x}(t) \tag{11}$$

$$\boldsymbol{C}_c = \begin{bmatrix} 1 & 0 \\ 0 & 1 \end{bmatrix} \tag{12}$$

Then, the discrete-time state-space equations are derived as given in (13)-(15) using T_s as the sampling time.

$$\boldsymbol{x}_m(k+1) = \boldsymbol{A}_m \boldsymbol{x}_m(k) + \boldsymbol{B}_m \boldsymbol{u}(k) + \boldsymbol{D}_m \boldsymbol{d}(k) \tag{13}$$

$$\boldsymbol{y}(k) = \boldsymbol{C}_m \boldsymbol{x}_m(k) \tag{14}$$

$$A_m = e^{A_c T_s} \ , \quad B_m = A_c^{-1}(e^{A_c T_s} - I)B_c \ , \ D_m = A_c^{-1}(e^{A_c T_s} - I)D_c \ , \ C_m = C_c \tag{15}$$

Differences of the state-space equations in (13) are:

$$\Delta x_m(k+1) = x_m(k+1) - x_m(k) = A_m \Delta x_m(k) + B_m \Delta u(k) + D_m \Delta d(k) \tag{16}$$

$\Delta \boldsymbol{x}_m$, $\Delta \boldsymbol{u}$ and $\Delta \boldsymbol{d}$ are differences of the states, inputs and disturbances, respectively. If the sampling time is sufficiently small, it can be assumed that the imposed voltages by the on-grid system have no large excursions during each time step and $\boldsymbol{\Delta d}(k) \approx \boldsymbol{0}$ for $k_i \le k \le k_i + N_c - 1$. Thus, the augmented state-space model is expressed as below:

$$X(k+1) = AX(k) + B\,\Delta u(k) \tag{17}$$

$$y(k) = CX(k) \tag{18}$$

$$X(k) = \begin{bmatrix} \Delta x_m(k) \\ y(k) \end{bmatrix}, \ A = \begin{bmatrix} A_m & 0 \\ C_m A_m & I \end{bmatrix}, B = \begin{bmatrix} B_m \\ C_m B_m \end{bmatrix}, C = \begin{bmatrix} 0 & I \end{bmatrix} \tag{19}$$

The objective function that is optimized for MPC is:

$$J = (R_s - Y)^T Q (R_s - Y) + \Delta U^T R \, \Delta U \tag{20}$$

where

$$Y = [y(k_i+1 \,|\, k_i) \quad \cdots \quad y(k_i+N_p \,|\, k_i)]^T = FX(k_i) + \Phi_B \Delta U$$

$$F = \begin{bmatrix} CA \\ CA^2 \\ \vdots \\ CA^{N_p} \end{bmatrix}, \quad \Phi_B = \begin{bmatrix} CB & 0 & & 0 \\ CAB & CB & & 0 \\ \vdots & \vdots & \cdots & \vdots \\ CA^{Np-1}B & CA^{Np-2}B & & CA^{Np-Nc}B \end{bmatrix} \tag{21}$$

$$\Delta U = \begin{bmatrix} \Delta u(k_i) \\ \vdots \\ \Delta u(k_i + N_c - 1) \end{bmatrix}, \quad R_s = \begin{bmatrix} I \\ I \\ \vdots \\ I \end{bmatrix} r(k_i), \quad r(k_i) = \begin{bmatrix} i_{dref}(k_i) \\ i_{qref}(k_i) \end{bmatrix}$$

$\Delta \boldsymbol{U}$ is differences of the control variables. k_i is the instant at which the control signals are produced for the future. N_p and N_c are prediction and control horizons, respectively. They are specified in the design process. $\boldsymbol{Q}$ and $\boldsymbol{R}$ are weighting diagonal matrices are so selected that the controller exhibits satisfactory performance. $i_{dref}(k_i)$ and $i_{qref}(k_i)$ are calculated as below:

$$i_{dref}(k_i) = i_{gd}^*(k_i) \tag{22}$$

$$i_{qref}(k_i) = i_{gq}^*(k_i) + C_f \omega v_o(k_i) \tag{23}$$

where $i_{gd}^*(k_i)$ and $i_{gq}^*(k_i)$ are obtained from (4) and (5) at instant k_i, respectively.

If a local load exists at PC of DER, with selecting set-points of i_d and i_q according to equations (22) and (23), local loads will draw their currents from the on-grid system. This matter will be an important problem when the local load is imbalanced or nonlinear which respectively leads to imbalance and distortion at the bus voltages as well as the PC voltages of DER. This bus voltage imbalance and distortion leads to ripple and distortion at exchanged power profiles. To provide local load by DER completely and to remove aforementioned undesired events, values of $i_{Ld}(k)$ and $i_{Lq}(k)$ must be added to $i_{dref}(k)$ and $i_{qref}(k)$ for $k_i \le k \le k_i + N_p$ as the set-points, respectively. If $i_{Ld}(k_i)$ and $i_{Lq}(k_i)$ as the references of the local load currents are added to $k_i \le k \le k_i + N_p$ (as conventional method in design of MPC), they lead to undesired performance for imbalanced, nonlinear and dynamic loads. To improve the performance of the MPC, and since $i_{Ld}(k)$ and $i_{Lq}(k)$ are unknown for $k_i \le k \le k_i + N_p$, these values are forecast for prediction horizon based on $i_{Ld}(k)$ and $i_{Lq}(k)$ in $0 \le k \le k_i$.

Moreover, if main grid voltage be imbalanced by each reason, v_{od} and v_{oq} will oscillate with 2ω-rad/sec sinusoidal ripple and according to (4)-(5) lead to oscillatory i_{gd}^* and i_{gq}^*. Thus choice of $\boldsymbol{R}_s$ according to (21) and allocating $i_{gd}^*(k_i)$, $i_{gq}^*(k_i)$ and $v_o(k_i) = \sqrt{v_d^2(k_i) + v_q^2(k_i)}$ to all of their set-points in the future instances cause undesired performance for the controller, and the powers are exchanged with oscillatory profiles and not smoothly. Thus, these values must be forecast for the better performance of the MPC with upstream grid voltage imbalance. As aforementioned, according to (17), if the sampling time T_s, be sufficiently small, this voltage imbalance does not affect the performance of the MPC and the forecasting $i_{gd}^*(k_i)$, $i_{gq}^*(k_i)$ and $v_o(k_i)$ are not required.

With respect to the above arguments

$$R_s = \begin{bmatrix} i_{dref}(k_i) \\ i_{qref}(k_i) \\ i_{dref}(k_i+1) \\ i_{qref}(k_i+1) \\ \vdots \\ i_{dref}(k_i+N_p) \\ i_{qref}(k_i+N_p) \end{bmatrix} = \begin{bmatrix} i_{gd}^*(k_i) + i_{Ld}(k_i) \\ i_{gq}^*(k_i) + C_f \omega v_o(k_i) + i_{Lq}(k_i) \\ i_{gd}^{*p}(k_i+1) + i_{Ld}^p(k_i+1) \\ i_{gq}^{*p}(k_i+1) + C_f \omega v_o^p(k_i+1) + i_{Lq}^p(k_i+1) \\ \vdots \\ i_{gd}^{*p}(k_i+N_p) + i_{Ld}^p(k_i+N_p) \\ i_{gq}^{*p}(k_i+N_p) + C_f \omega v_o^p(k_i+N_p) + i_{Lq}^p(k_i+N_p) \end{bmatrix} \tag{24}$$

where $i_{gd}^{*p}(k_i)$, $i_{gq}^{*p}(k_i)$, $i_{Ld}^p(k_i)$ and $i_{Lq}^p(k_i)$ are predicted values of $i_{gd}^*(k_i)$, $i_{gq}^*(k_i)$, $i_{Ld}(k_i)$ and $i_{Lq}(k_i)$, respectively. These values are obtained by linear extrapolation technique.

$\Delta \boldsymbol{U}$ is obtained as below by minimizing the objective function in (20):

$$\Delta U = (\Phi_B^T Q \Phi_B + R)^{-1} \Phi_B^T Q (R_s - FX(k_i)) \tag{25}$$

Based on receding horizon principle

$$\Delta u(k_i) = \overbrace{\begin{pmatrix} I & 0 & \cdots & 0 \end{pmatrix}}^{Nc} \Delta U = K_y \, r(k_i) - K_{mpc} \, X(k_i) = K_y(r(k_i) - y(k_i)) - K_x \Delta x_m(k_i) \tag{26}$$

$\boldsymbol{K}_y$, $\boldsymbol{K}_x$ and $\boldsymbol{K}_{mpc} = [\boldsymbol{K}_x \ \boldsymbol{K}_y]$ are coefficient matrices. The discrete-time MPC block diagram with set-point forecasting path is shown in Fig. 4.

4- 2- Stability analysis

MPC has been widely applied as an effective control strategy for many industrial applications, and its stability has also been under study [32]. There are some studied cases in the literature to establish the stability of MPC such as stability of MPC with terminal-state constraints, stability of MPC

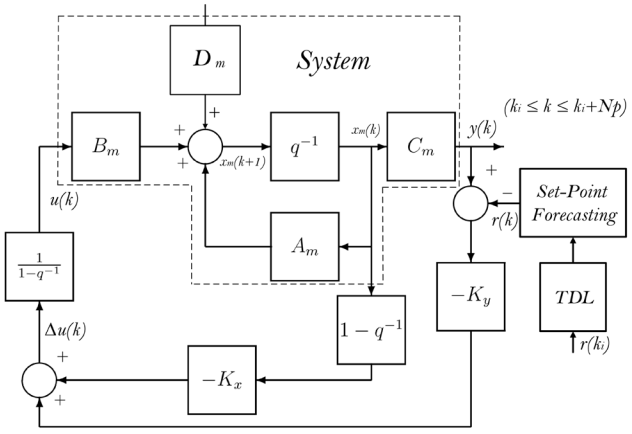

Fig. 4. The discrete-time MPC block diagram with set-point forecasting path

with sufficiently large prediction horizon (or infinite horizon) and stability of MPC with terminal-state penalty in the cost function [30], [33] and [34]. In this paper, the finite receding horizon MPC (often called classic MPC [35]) with a cost function given in (20) where does not have terminal-state constraints and terminal-state penalty is used to achieve desirable performance of the DG main controller. An approach based on the Lyapunov function was given in [35] to establish the stability of the classic MPC where the model of the controlled system is perfect. The perfect model as defined in [35] is the system model without disturbances. The key point is to find a Lyapunov function for the MPC.

To analyze stability of the proposed controller, a similar approach as given in [35] is used. Thus, (26) is rewritten as below:

$$\Delta u(k) = -K_{mpc}\tilde{X}(k) \tag{27}$$

where

$$\tilde{\mathbf{X}}(k) = \begin{bmatrix} \Delta \mathbf{x}_m(k) \\ \mathbf{y}(k) - \mathbf{r}(k) \end{bmatrix}.$$

The closed-loop state-space equations of system are given in (28).

$$\tilde{X}(k+1) = A\tilde{X}(k) + B\Delta u(k) = (A - BK_{mpc})\tilde{X}(k) \tag{28}$$

The cost function given in (20) can be rewritten as (29) for the system that will be similar to the cost function of a discrete-time linear quadratic regulator (DLQR).

$$J = \sum_{m=1}^{Np} \tilde{X}^T(k+m|k)\tilde{Q}\tilde{X}(k+m|k) + \sum_{m=0}^{Nc-1} \Delta u^T(k+m|k)\bar{R}\Delta u(k+m|k) \tag{29}$$

where $\tilde{Q} = \begin{bmatrix} \mathbf{0} & \mathbf{0} \\ \mathbf{0} & \bar{Q} \end{bmatrix}$.

$\bar{Q}_{2\times2}$ and $\bar{R}_{2\times2}$ are coefficient submatrices that are located on the main diagonals of $\boldsymbol{Q}$ and $\boldsymbol{R}$, respectively. The Lyapunov function $V(\tilde{\boldsymbol{X}}\ (k), k)$ is chosen as below:

$$V(\tilde{X}(k),k) = J_{\min} = \sum_{m=1}^{Np} \tilde{X}^{*T}(k+m|k)\tilde{Q}\tilde{X}^*(k+m|k) + \sum_{m=0}^{Nc-1} \Delta u^{*T}(k+m|k)\bar{R}\Delta u^*(k+m|k) \tag{30}$$

Superscript * denotes the optimal values. The stability of the classic MPC is established when the Lyapunov function decreases along the state trajectory:

$$V(\tilde{X}\ (k+1), k+1) - V(\tilde{X}\ (k), k) < 0 \tag{31}$$

Using the proved theorem given in [35], the closed-loop system of the classic MPC is stable and (31) is met when there exists any $\Delta u^*(k)$ such that:

$$\tilde{X}^{*T}(k+1|k)\tilde{Q}\tilde{X}^*(k+1|k) - \tilde{X}^T(k|k)\tilde{Q}\tilde{X}(k|k) + \Delta u^{*T}(k|k)\bar{R}\Delta u^*(k|k) < 0 \tag{32}$$

Using (28) and (32), the following condition can be obtained:

$$\begin{aligned} &(A - BK_{mpc})^T \tilde{Q}(A - BK_{mpc}) + K_{mpc}{}^T \bar{R}K_{mpc} - \tilde{Q} < 0 \\ &K_{mpc} = \underbrace{\begin{bmatrix} I_{2\times2} & 0_{2\times2} & \cdots & 0_{2\times2} \end{bmatrix}}_{Nc} (\Phi_B^T Q \Phi_B + R)^{-1} \Phi_B^T Q F \end{aligned} \tag{33}$$

Therefore, if $\bar{Q}$ and $\bar{R}$ are selected appropriately such that (33) is met, the stability of the proposed controller will be guaranteed. For instance, the stability is guaranteed for chosen $\bar{Q} = I_{2\times2}$ and $\bar{R} = I_{2\times2}$ where N_p=N_c=20.

5- Time-domain simulation results

In this section, the proposed control scheme is applied to a grid-connected DER with a capacity of 10 *MVA* and its performance is investigated under various case studies. The detailed switched model of the system is simulated using PSCAD/EMTDC [31]. A collection of different local load types is considered to be connected to the PC through individual circuit breakers as shown in Fig. 2. The local loads include: (a) two three-phase balanced loads, (b) an induction motor, (c) an imbalanced load and (d) a nonlinear load. In figures and tables, voltages are expressed in *kV*, currents in *kA*, active (reactive) power in *MW* (*MVAr*), load torque in per-unit (*p.u.*). For the local load collection, four case studies are examined where the open/close state of breakers and set-points of active and reactive powers are given in tables in specified time intervals. Also the performance of the proposed control scheme under unbalance voltages of main grid is demonstrated in a case study. In these case studies obtained results are compared with those of PI-based scheme proposed in [6] and CMPC (conventional MPC) scheme. In case study 1 to 7, one DG is considered that is connected to the main grid. The last case study is related to connection and parallel operation of three DERs in a grid-connected multi-bus MG shown in Fig. 1. In all case studies the renewable energy resources are replaced with DC voltage sources, thus the dynamics of them are not considered.

5- 1- Case study 1: Three-phase balanced local load

Two three-phase balanced loads are connected to and disconnected from the PC in a sequence given in Table 2. Simulation results are illustrated in Fig. 5 for the proposed control scheme. As can be observed, active and reactive powers are exchanged very fast and accurately even after each switching instant. Waveforms for two other schemes (PI and CMPC) are the same as those have been shown in Fig. 5 and the schemes have no superiority to each other.

Table 2. Case study 1

time [s]	0-0.1	0.1-0.25		0.25-0.35	0.35-0.45	0.45-0.55	0.55-0.8
B1_1	O	O		C	C	C	O
B1_2	O	O		O	C	O	O
time [s]	0-0.1	0.1-0.3	0.3-0.4	0.4-0. 5	0.5-0.6	0.6-0.7	0.7-0.8
P_g	0	5	1	3	2	-2	0
Q_g	0	0	0	1	-2	0	0

O = open, C = close, P [MW], Q [MVAr]

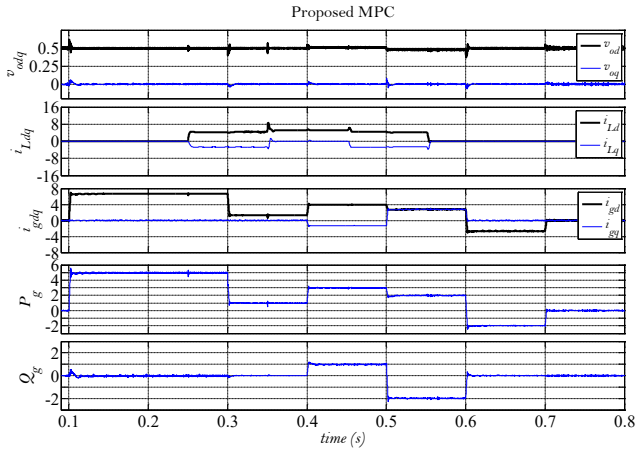

Fig. 5. The results of the proposed control scheme in case study 1.

5- 2- Case study 2: Three-phase imbalanced local load

The three-phase imbalanced load is connected (B3 is closed) to the PC from t= 0.2 s and is followed by several changes in set-points of active and reactive powers as given in Table 1. This load (R_3=1 [mΩ] and L_3=3 [μH]) is selected greater (about 7 times) than that presented in Table 1. Fig. 6 to 8 illustrate the results of three control schemes. A comparison of the results is illustrated in Fig. 9. In Fig.9 (a) to (c) waveforms of the injected currents to the upstream grid are shown. As

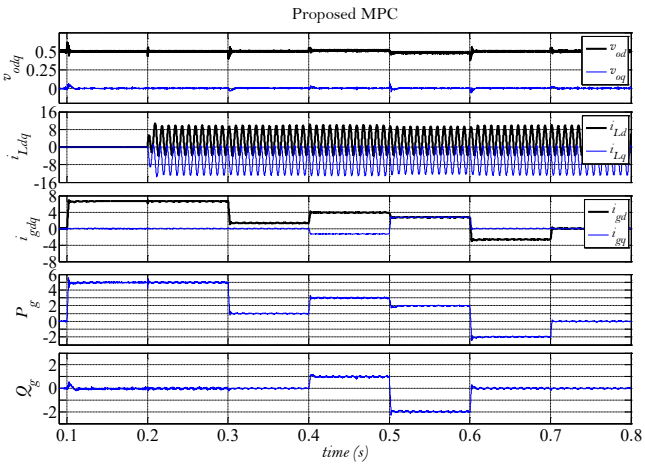

Fig. 6. The results of the proposed control scheme in case study 2.

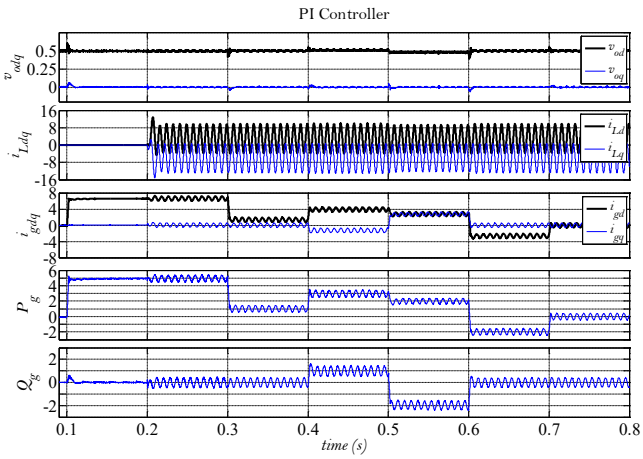

Fig. 7. The results of the PI-based control scheme in case study 2.

can be seen, injected currents when proposed scheme is used are pure sinusoidal balanced currents. The better steady-state performance of the proposed scheme is clearly observed. When the imbalanced load is connected to the PC at t=0.2 s, P_g and Q_g are distorted by 2ω rad/sec ripple components for the PI-based control scheme and CMPC due to portion of imbalanced local load currents i_{Labc} drawn from main grid. Such ripples are very little in P_g and Q_g for the proposed control scheme, and exchanged powers are very smooth (see Fig. 9(d) and (e)). As Fig. 6 to 8 shown, the performance of the PI-based is better than CMPC, but the proposed control scheme demonstrates much desired performance in comparison with two other schemes.

5- 3- Case study 3: Nonlinear and imbalanced local load

The same sequence of events as the case study 2 is considered for this study where addition to B3, B4 is also closed at t=0.2 s. In this case study, R_4=300 [mΩ] and L_4=10 [μH] are greater than those in Table 1. Fig. 10, 11 and 12 illustrate the obtained results of three control schemes. Although the three schemes can successfully regulate the powers to their set-points, the steady state performance of the proposed scheme is much better as can be observed in Fig. 13.

5- 4- Case study 4: Induction motor starting

The effectiveness of the proposed scheme is studied for starting an induction motor. The sequence of events is given in

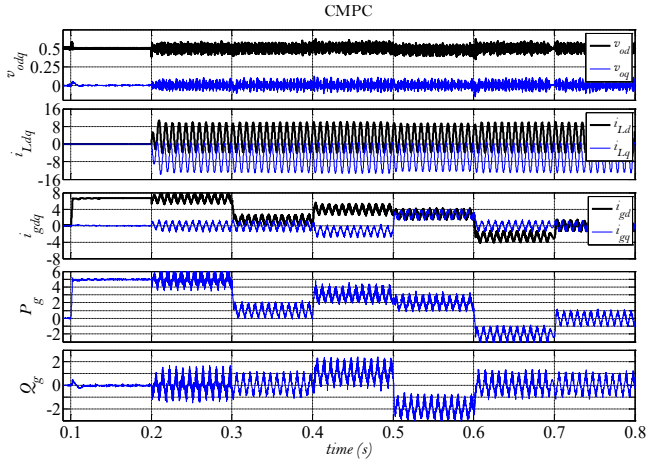

Fig. 8. The results of the CMPC in case study 2.

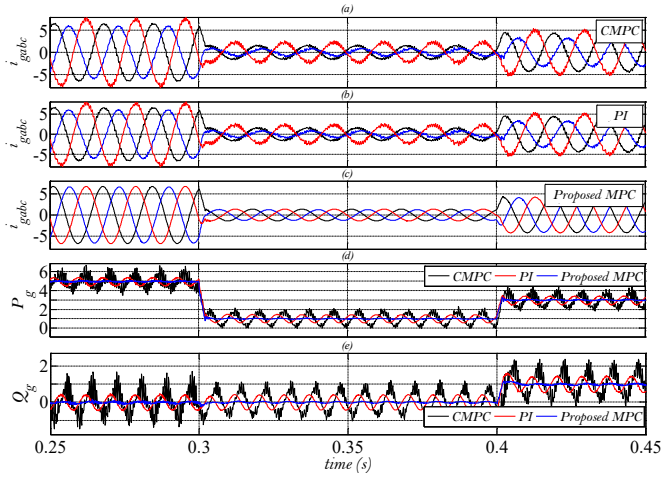

Fig. 9. Comparison of the results: (a)-(c): injected currents to upstream grid, (d) and (e): exchanged active and reactive powers when CMPC, PI-based controller and proposed MPC are used in case study 2.

Table 3. Fig. 14, 15 and 16 illustrate the results of three control schemes. As can be seen, the proposed control scheme regulates active and reactive powers accurately. However, the PI-based scheme and CMPC have similar performance for this load condition and cannot properly regulate active and reactive powers. In Fig. 17 the exchanged power for PI-based and the proposed schemes are compared and the superiority of the proposed scheme is evident.

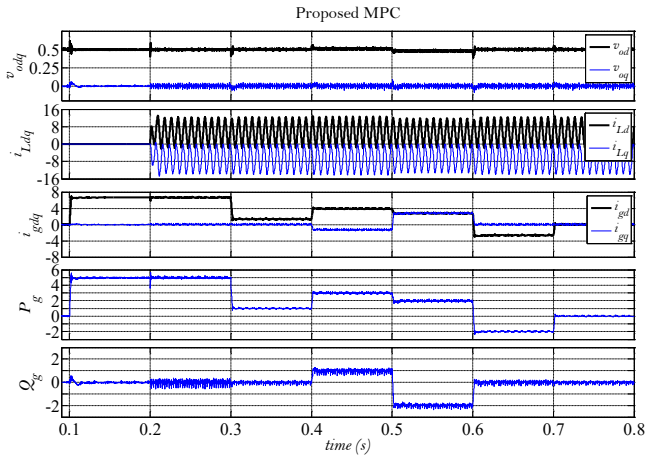

Fig. 10. The results of the proposed control scheme in case study 3.

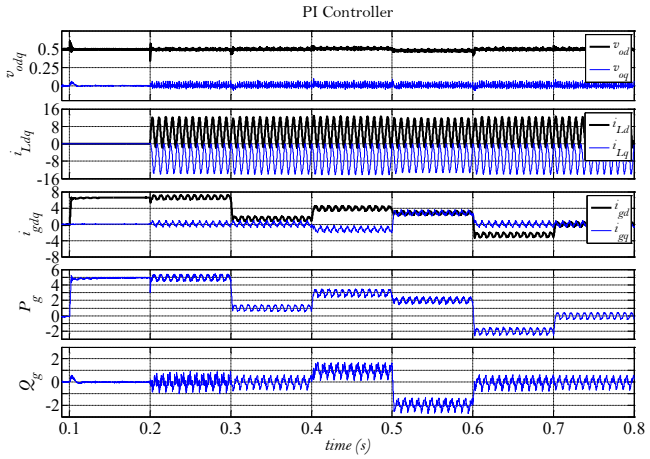

Fig. 11. The results of the PI-based control scheme in case study 3.

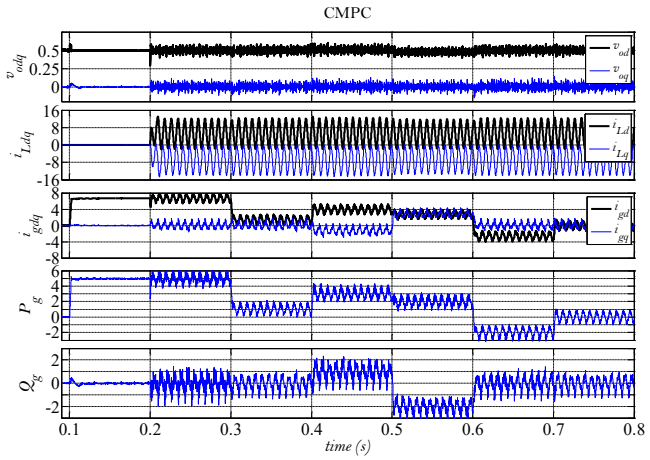

Fig. 12. The results of the CMPC in case study 3.

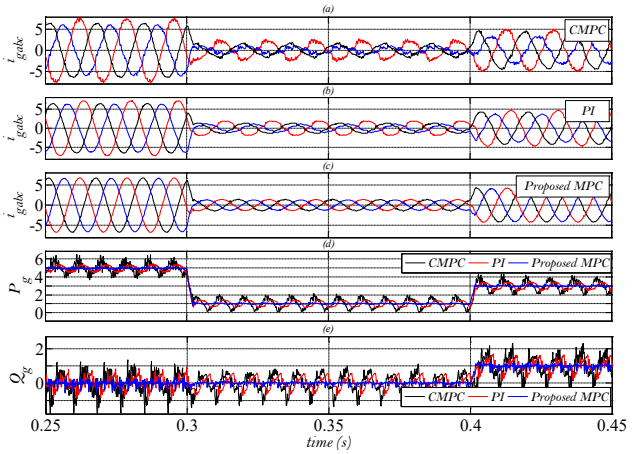

Fig. 13. Comparison of the results: (a)-(c): injected currents to upstream grid, (d) and (e): exchanged active and reactive powers when CMPC, PI-based controller and proposed MPC are used in case study 3.

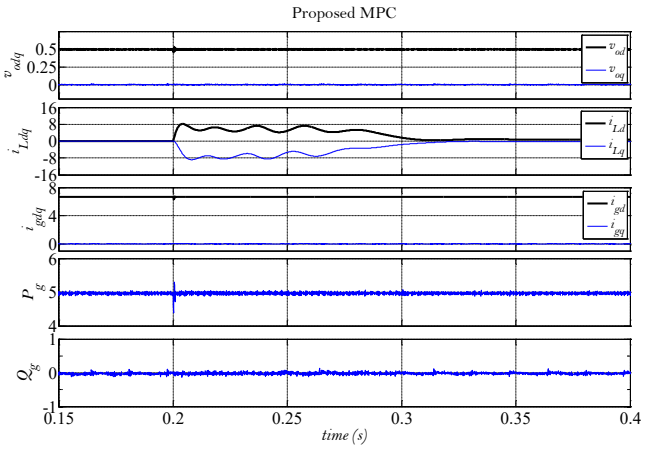

Fig. 14. The results of the proposed control scheme

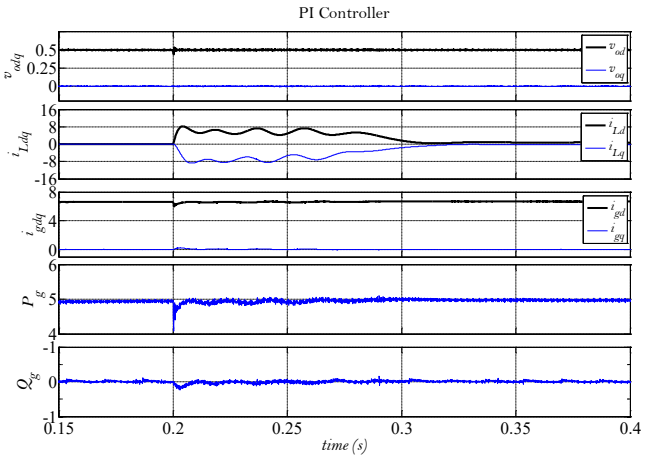

Fig. 15. The results of the PI-based control scheme in case study 4.

Table 3. Case study 4

time [s]	0-0.2	0.2-0.4
B2	O	C
T_L	0	0.7
Pg	5	5
Qg	0	0

O = open, C = close, P [MW], Q [MVAr]

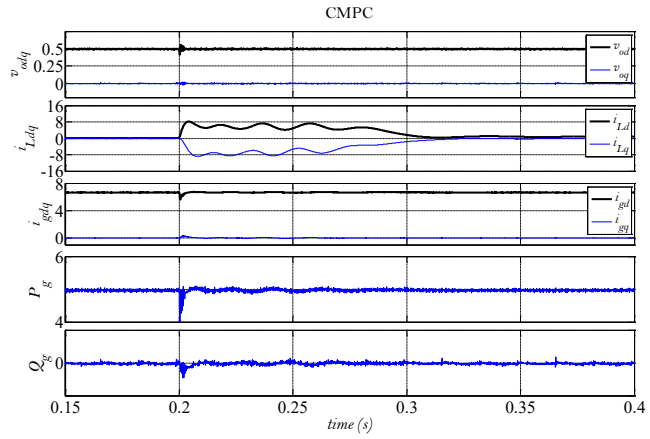

Fig. 16. The results of the CMPC in case study 4.

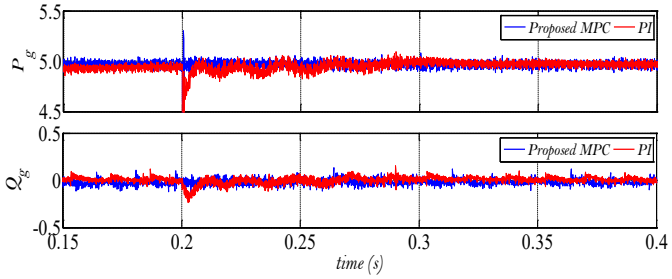

Fig. 17. Comparison of the results of the proposed and PI-based schemes in case study 4.

5- 5- Case study 5: Main grid voltage imbalance

The same sequence of power set-points as the case study 2 is considered for the case study 5. The imbalanced local load is connected to the PC at t=0.5 s. Main grid voltages are imbalanced. Therefore v_{od} and v_{oq} will oscillate with 2ω-rad/sec sinusoidal ripple and lead to oscillatory $i_{gd}^*$and i_{gq}^*. Fig. 18, 19 and 20 illustrate the obtained results of the three control schemes. Although the schemes can successfully regulate powers to their set-points, the steady state performance of the proposed scheme is much better, as can be observed in Fig. 21. As mentioned in section 4, when local load is not connected yet (up to t=0.5 s), since the sampling time in the simulation is selected sufficiently small, the profiles of the exchanged active (reactive) power when the proposed control

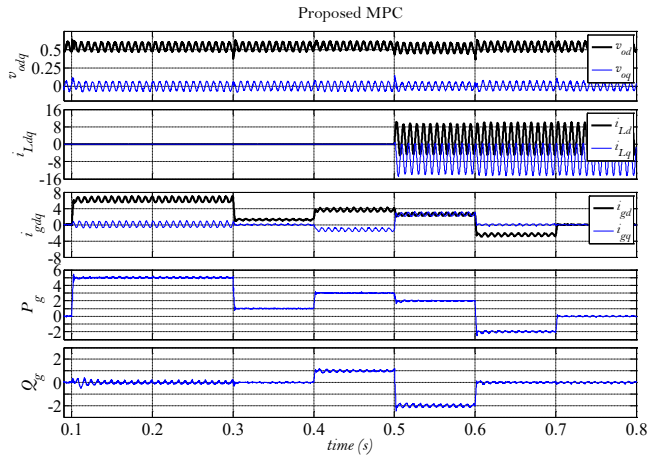

Fig. 18. The results of the proposed control scheme in case study 5.

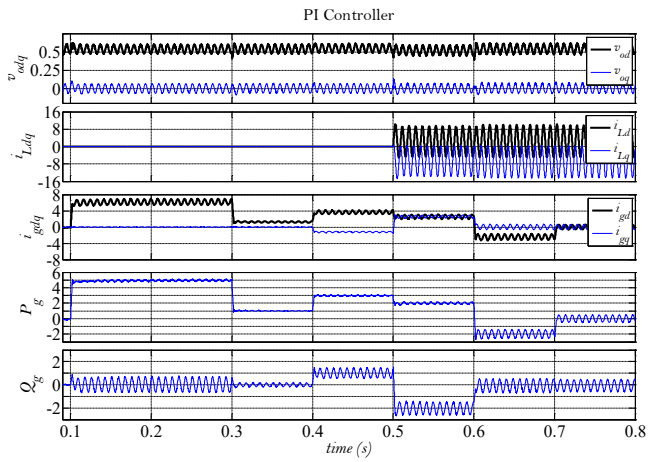

Fig. 19. The results of the PI-based control scheme in case study 5.

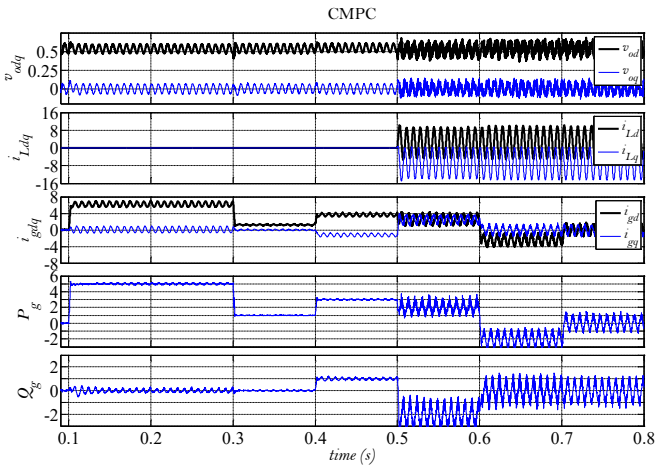

Fig. 20. The results of the CMPC in case study 5.

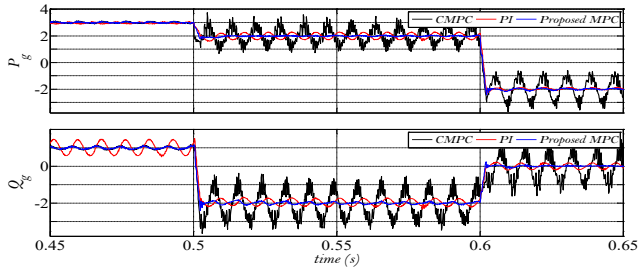

Fig. 21. Comparison of the results of three schemes in case study 5

scheme and CMPC are utilized is similar to each other and are smoother than those of PI-based scheme, but when the local load is connected (after t=0.5 s), CMPC has no desired performance in comparison with the proposed and PI-based control schemes(see Fig. 21).

5- 6- Case study 6: Robustness Assessment

In practical applications, system parameters like R, L_f and C_f are subjected to some uncertainties. To assess the robustness of the proposed control scheme, -50% mismatch in L_f and C_f and +100% mismatch in R are supposed and the case study 2 is repeated. As depicted in Fig. 22, the results show stable

performance of the proposed scheme and accurate regulation of exchanged active (reactive) power under the assumed uncertainties.

5- 7- Case study 7: Measurement noises

In this case study, case study 2 is repeated by considering measurement noises. Measurement noises with 20 percent value [36] are supposed for currents in measurement process. Fig. 23 shows the performance of the proposed controller and compares the power profiles with those of case study 2, where no measurement noises exist.

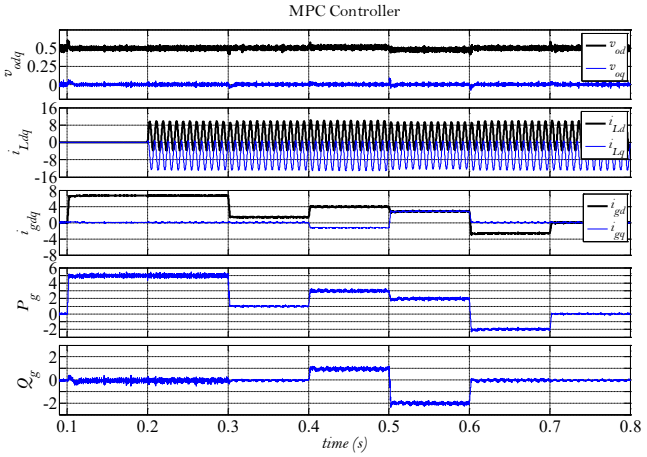

Fig. 22. The results of the proposed control scheme in case study 6.

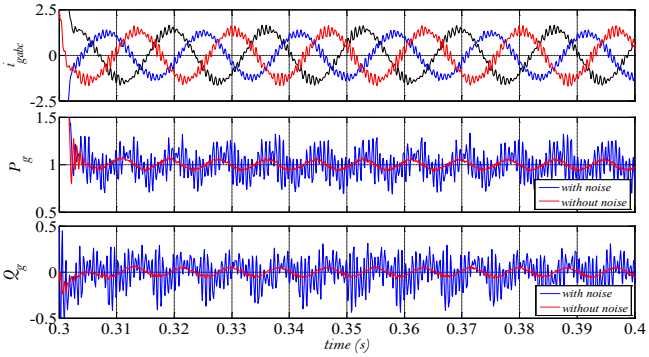

Fig. 23. Zoomed view of the proposed control scheme results in case study 7.

5- 8- Case study 8: Grid-connected operation of a multi-bus MG

In this case study MG described in section 2 is studied. The considered scenario and sequence of events are given in Table 4. MG must provide 6 *MW* for the main grid during the scenario. DGs in addition to powers that deliver to the MG, must provide their local load. Therefore, as aforementioned, active power set-points of DGs which are positive or zero values are dependent on the obtained data from MPPT mechanism (total producible power) and are required active power of their local loads. Those for BT are determined by power balance equation (1) which can be positive or negative or zero. Reactive power set-points are determined based on MG internal consumption and grid operator command. Fig. 24 to Fig. 26 show simulation results for DERs in the MG under given scenario. As can be seen, powers are exchanged very smoothly under various events. At t=0.75 s, the substation imbalanced load is connected, and due to imbalanced currents which draws from main transformer voltage at low voltage side, is imbalanced. This unbalancing is propagated to PC voltages of DERs (v_{odq} oscillate from t=0.75 s). Delivered powers by DERs under this event are approximately maintained smooth, but aggregated power injected to the main grid through the main transformer has small amplitude sinusoidal ripple (see Fig. 27). If PI-based control scheme or CMPC is used, aggregated powers delivered will have severe ripples under the given scenario.

Table 4. Case study 8

time [s]	0.1-0.2	0.2-0.3	0.3-0.4	0.4-0.5	0.5-0.6	0.6-0.7	0.7-0.75	0.75-1
$B3_{DERs}$ (local load)	C	C	C	C	C	O	C	C
S_c (common load)	O	O	C	C	C	O	O	O
S_{sub} (substation load)	O	O	O	O	O	O	O	C
P_{DER1}	3	3	2	2	5	3	3	3
P_{DER2}	3	1	1	5	5	5	1.25	1.25
P_{DER3}	0.13	2.13	4.55	0.57	-2.33	-1.81	1.88	1.88
P_{demand}	6	6	6	6	6	6	6	6
$P_{common\ load}$	0	0	1.4	1.4	1.4	0	0	0
P_{loss}	0.13	0.13	0.15	0.17	0.27	0.2	0.13	0.13
Q_{DERs}	0.5	0.5	0.8	0.8	0.8	0.5	0.5	0.5

O = open, C = close, P [MW], Q [MVAr]

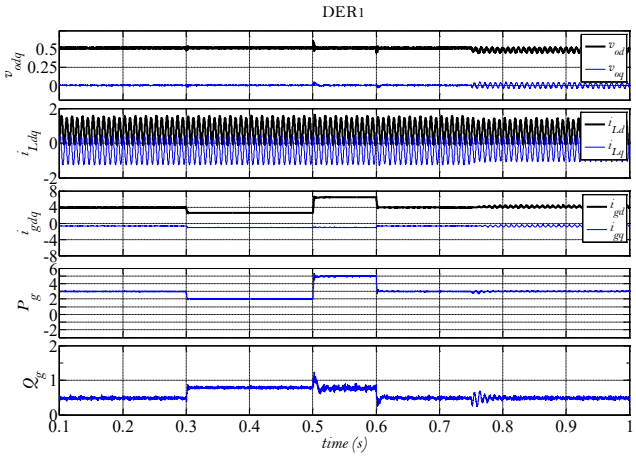

Fig. 24. The results of DER1 for the proposed control scheme in case study 8.

6- Conclusions

A control scheme based on MPC is proposed for the main controller of inverter-based DERs to regulate active and reactive powers exchanged between DERs and on-grid system. Active and reactive power control change to current control and the set-points are forecast to improve DER

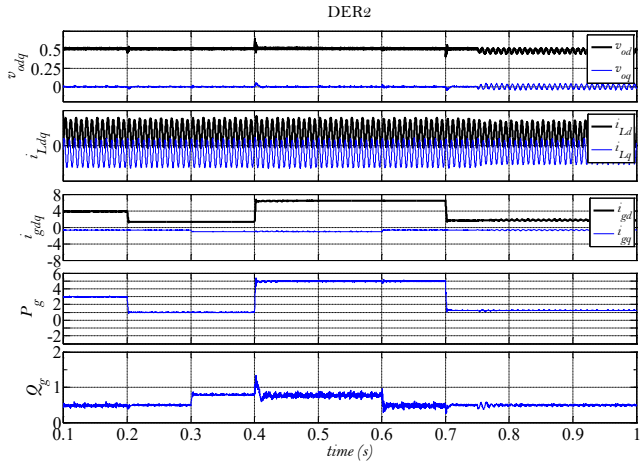

Fig. 25. The results of DER2 for the proposed control scheme in case study 8.

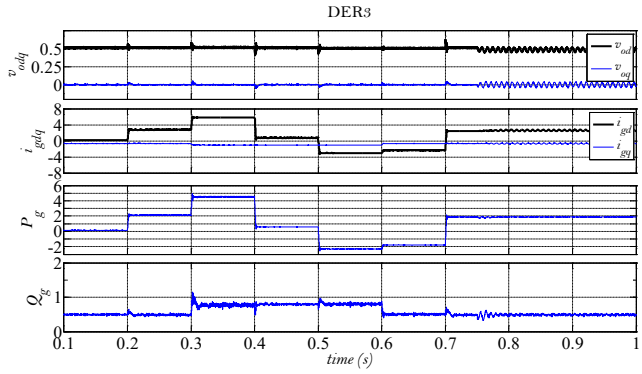

Fig. 26. The results of DER3 for the proposed control scheme in case study 8.

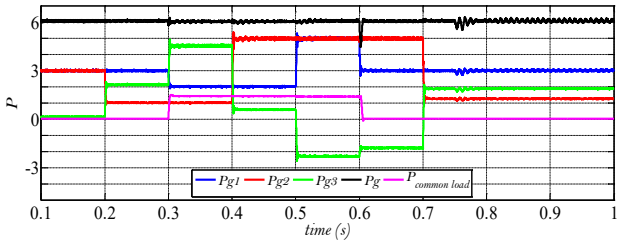

Fig. 27. Power profiles in case study 8.

performance under various types of local loads and voltage imbalance of the main grid. While imbalanced/nonlinear and induction motor loads as local loads are switching or bus voltages are imbalanced, the regulation is performed properly and smoothly. The control scheme enables an accurate active/reactive power regulation in connecting the DER to a multi-bus grid-connected MG in parallel operation with other DERs. The proposed control scheme presents much better performance in comparison with the PI-based control scheme and CMPC.

References

[1] G. Pepermans, J. Driesen, D. Haeseldonckx, R. Belmans, W. Dhaeseleer, Distributed generation: Definition, benefits and issues, Energy Policy, 33(6): (2005) 787–98.

[2] T. C. Green, M. Prodanovic, Control of inverter-based micro-grids, Electr. Power Syst. Res. Distrib. Generation, 77(9) (2007) 1204–13.

[3] J. Rocabert, A. Luna, F. Blaabjerg, P. Rodriguez, Control of Power Converters in AC Microgrids, IEEE Trans. on Power Electronics, 27(11) (2012) 4734-4749.

[4] F.A. Bhuiyan, A. Yazdani, Energy Storage Technologies for Grid-Connected and Off-Grid Power System Applications, IEEE Electrical Power and Energy Conference, 2012.

[5] A. Deihimi, B. Keshavarz Zahed, R. Iravani, An interactive operation management of a micro-grid with multiple distributed generations using multi-objective uniform water cycle algorithm, Energy, 106 (2016) 482-509.

[6] A. Yazdani, R. Iravani, Voltage-Sourced Converters in Power Systems: modeling, control and applications, IEEE Wiley Press, 2010.

[7] L. Shang, J. Hu, Sliding-mode-based direct power control of grid-connected wind-turbine-driven doubly fed induction generators under unbalanced grid voltage conditions, IEEE Trans. Energy Conversion, 27(2) (2012) 362–373.

[8] L. Shang, D. Sun, J. Hu, Sliding-mode-based direct power control of grid-connected voltage-sourced inverters under unbalanced network conditions, IET Power Electron, 4(5) (2011) 570–579.

[9] M.M, Rezaei, J. Soltani, A robust control strategy for a grid-connected multi-bus microgrid under unbalanced load conditions, Electrical Power and Energy Systems, 71 (2015) 68-76.

[10] M. Mehrasa, E. Pouresmaeil, B. N. Jørgensen, J. P.S. Catalão, A control plan for the stable operation of microgrids during grid-connected and islanded modes, Electric Power Systems Research, 129 (2015) 10-22.

[11] A. H. Syed, M.A. Abido, New enhanced performance robust control design schemefor grid-connected VSI, Control Engineering Practice, 53 (2016) 92-108.

[12] E. Pouresmaeil, O. Gomis-Bellmunt, D. Montesinos-Miracle, J. Bergas-Jané, Multilevel converters control for renewable energy integration to the power grid, Energy, 36 (2011) 950-363.

[13] J. Hu, J. Zhu, D. G. Dorrell, Model predictive control of inverters for both islanded and grid-connected operations in renewable power generations, IET Renewable Power Generation, 8(3) (2013) 240-248.

[14] V. Yaramasu, B. Wu, Model predictive decoupled active and reactive power control for high-power grid-connected four-level diode-clamped inverters, IEEE Trans. Power Electron, 61(7) (2014) 3407–3417.

[15] R. Halvgaard, L. Vandenberghe, N.K. Poulsen, H. Madsen, J.B. Jørgensen, Distributed model predictive control for smart energy systems, IEEE Trans. Smart Grid, 7(3) (2016) 1675-1682.

[16] A.S. Ashtari, A. Khaki Sedigh, Adaptive Simplified Model Predictive Control with Tuning Considerations, Amirkabir International Journal of Science& Research, 46(2) (2014).

[17] P. Kou, D. Liang, L. Gao, F. Gao, Stochastic coordination of plug-In electric vehicles and wind turbines in microgrid: a model predictive control approach, IEEE Trans. Smart Grid, 7(3) (2016) 1537-1551.

[18] J. Rodriguez, P. Cortes, Predictive Control of Power Converters and Electrical Drives, IEEE Wiley Press, 2012.

[19] L. Tarisciotti, P. Zanchetta, A. Watson, S. Bifaretti, J. C. Clare, Modulated model predictive control for a 7- level cascaded H-bridge back-to-back converter, IEEE Trans. Ind. Electron, 61(2) (2014) 5375-5383.

[20] K. M. Abo-Al-Ez, A. Elaiw, X. Xia, A dual-loop model predictive voltage control/sliding-mode current control for voltage source inverter operation in smart microgrids, Electric Power Components and Systems, 42(3) (2014) 348-360.

[21] P. Cortés, G. Ortiz, J. I. Yuz, J. Rodriguez, S. Vazquez, L. G. Franquelo, Model predictive control of an inverter with output LC filter for UPS applications, IEEE Trans. Ind. Electron, 56(6) (2009) 1875-1883.

[22] K. T. Tan, X. Y. Peng, P. L. So, Y. C. Chu, M. Z. Q. Chen, Centralized Control for Parallel Operation of Distributed Generation Inverters in Microgrids, IEEE Trans. On Smart Grid, 3(4) (2012) 1977-1987.

[23] D. Song, J. Yang, M. Dong, Y. H. Joo, Model predictive control with finite control set for variable-speed wind turbines, Energy, Accepted Manuscript (2017).

[24] M. Hamzeh, H. Karimi, H. Mokhtari, Harmonic and Negative-Sequence Current Control in an Islanded Multi-Bus MV Microgrid, IEEE Trans. On Smart Grid, (2013).

[25] S. K. Chung, A phase tracking system for three phase utility interface inverters, IEEE Transactions on Power Electronics, 5(3) (2000) 431-438.

[26] A. Medjber, A. Guessoum, H. Belmili, A. Mellit, New neural network and fuzzy logic controllers to monitor maximum power for wind energy conversion system, Energy, 106 (2016) 137-146.

[27] S. Ganjefar, A. Mohammadi, Variable speed wind turbines with maximum power extraction using singular perturbation theory, Energy, 106 (2016) 510-519.

[28] M. E. Basoglu, B. Çakir, A novel voltage-current characteristic based global maximum power point tracking algorithm in photovoltaic systems, Energy, 112 (2016) 153-163.

[29] S. S. Mohammed, D. Devaraj, T.P. I. Ahamed, A novel hybrid Maximum Power Point Tracking Technique using Perturb & Observe algorithm and Learning Automata for solar PV system, Energy, 112 (2016) 1096-1106.

[30] L. Wang, Model Predictive Control System Design and Implementation Using MATLAB, London, 2009.

[31] PSCAD/EMTDC v. 4.5.0.0, Manitoba HVDC Research Centre, Winnipeg, MB, Canada, 2012.

[32] J. Lofberg, Linear Model Predictive Control Stability and Robustness, Sweden, 2001.

[33] L. Grune, J. Pannek, Nonlinear Model Predictive Control: Theory and Algorithems, Springer Press 2017.

[34] J. M. Maciejowski, Predictive Control with Constraints, London, 2000.

[35] W. H. Chen, Stability Analysis of Classic Finite Horizon Model Predictive Control, International Journal of Control, Automation and Systems, 8(2) (2010) 187-197.

[36] N. Suyaroj, N. Watson, Transients State Estimation with Measurement Noise, IEEE Conference, 2015.

Please cite this article using:

A. Saleh, A. Dehimi, Model Predictive Control of Distributed Energy Resources with Predictive Set-Points for Grid-Connected Operation, *AUT J. Elec. Eng.*, 50(2) (2018) 109-120.

DOI: 10.22060/eej.2018.14303.5217